approach, the effects of which become trivial when absorption and a Gaussian smoothed incident plane wave are introduced, since both damp the wave field near two ends of each slice to zero, so that the periodic boundary interference becomes negligible.

For the edge area of the vacuum part of each unit cell, each multislice iteration is equivalent to adding a constant phase term to the incident tilted plane wave in the same area. We may therefore always repair this edge area by replacing it with the corresponding edge area of a tilted incident plane wave as long as the wave function in this area is multiplied by a proper phase term which can be easily calculated. Thus the small limited patched edge area in fact plays the role of an infinite plane-wave source which is crucial for obtaining a stationary solution for RHEED. It should be pointed out that it is not necessary to repair the deteriorated edge often because the moving edge seriously deteriorates the solution only after a certain number of iterations. Therefore, the computation time does not increase significantly due to the 'repairing'. The rate of deterioration of the edge depends primarily upon two parameters, the incident angle (θ_0) and the slice thickness (Δz), and the frequency of repairing can be made self-adjustable in the program.

Fig. 1(i) shows the results calculated for the 2×1 missing row reconstruction on the Au(001) surface. All calculation conditions are the same as those for Fig. 2(i) in our previous paper (Ma & Marks, 1990), except that the edge-patching method is used and 2050 iterations are calculated here. The surface is set at B and 3/4 of each slice on the left (from A to B) contains the vacuum wave and 1/4 of each slice on the right (from B to C) contains the crystal wave. The beam direction is along [010]. The calculation thickness is much thicker than that previously used, up to 2075·5 Å. It is infinite theoretically. The last four slices in Fig. 1(i) demonstrate that the stationary solution for the 2×1 Au(001) surface has been obtained. The patched edge area only shows the tilted plane-wave component when the stationary solution gradually forms in the non-patched-edge area. Since the wave front of the Bragg reflected waves always moves away from the crystal, the discontinuity between these two areas will not affect the final solution as long as the continuity of the incident-plane-wave components in these two areas is well preserved. Fig. 1(ii) shows the RHEED patterns corresponding to Fig. 1(i). They are Fourier transforms of the vacuum waves excluding the patched area in the slices in Fig. 1(i). The incident beam has been cut off. The reconstruction spots and spots corresponding to the double period on the 2×1 Au(001) surface (03) have emerged in the stationary solution shown in the last four patterns.

This work was supported by the National Science Foundation, Grant no. DMR 85-20280 and DMR 87-17376. The author is very grateful for many useful discussions with Professor L. D. Marks about this work.

References

COWLEY, J. M. & MOODIE, A. F. (1959). *Acta Cryst.* **12**, 353-359.
MA, Y. & MARKS, L. D. (1990). *Acta Cryst.* A**46**, 594-606.
PENG, L. M. & COWLEY, J. M. (1986). *Acta Cryst.* A**42**, 545-552.

Acta Cryst. (1991). A**47**, 139-142

Observation of nonprojective moiré fringe patterns produced with an X-ray interferometer.

By J. YOSHIMURA, *Institute of Inorganic Synthesis, Faculty of Engineering, Yamanashi University, Kofu* 400, *Japan*

(*Received* 6 *December* 1989; *accepted* 12 *September* 1990)

Abstract

Moiré fringes produced with an X-ray interferometer have been found to give an extraordinary nonprojectiveness, an oscillatory change of the fringe position along the beam paths of the transmitted and the Bragg reflected waves behind the interferometer. Densitometric measurements of the moiré fringes showed that, along with the fringe position, the fringe profile changes in an unusual manner along the beam paths. This nonprojectiveness is presumably of the same nature as that observed for moiré fringes produced with a bicrystal [Yoshimura (1989). *J. Phys. Soc. Jpn*, **58**, 1283-1295].

In recent papers (Yoshimura, 1987, 1989), it has been shown that X-ray moiré fringes observed with a bicrystal specimen are not exactly the projection of the intensity distribution of the wave field on the exit surface of the crystal, but do oscillate along the beam paths behind the crystal. This nonprojectiveness of moiré fringes is inexplicable by the current theory of moiré fringes (*cf.* Yoshimura, 1989) and therefore is of interest. In this paper we report a similar fringe oscillation observed for moiré fringes produced with an X-ray interferometer. The present moiré fringes are nearly a parallel moiré pattern while the previous ones were nearly a rotation moiré pattern.

The experimental set-up was basically the same as before [see Fig. 1 in Yoshimura (1989)]. X-ray topographs of moiré patterns were taken with a double-crystal arrangement in the parallel setting for Si 220 reflection with Mo $K\alpha$ radiation. An asymmetrically cut collimator crystal was used so as to make the angular spread of the incident beam on the specimen 0·45″. A standard *LLL*-type X-ray interferometer (Bonse & Hart, 1965), about 26 mm long and 25 mm wide, was mounted on the specimen position instead of the bicrystal. The surfaces of the three components of the X-ray interferometer were parallel to (111), and their thicknesses were 0·8 mm. To produce moiré patterns, a point on the top of the analyzer wafer was locally heated. Very thin Pt wires stretched in a frame were placed between the specimen and X-ray films so that their shadow images gave a standard for position and/or orientation on the topographs. Moiré patterns were recorded simultaneously on three to seven X-ray films placed at different distances

0108-7673/91/020139-03$03.00

from the specimen. Exposure time was 30–50 min. For these moiré-pattern recordings, single-sided X-ray films were especially prepared from Fuji no. 150 films. The emulsion thickness was 10 μm. Intensity attenuation of X-rays through each film was 6·9%.

Fig. 1 shows examples of moiré patterns recorded simultaneously on seven films placed parallel to one another but at different distances from the specimen. The spacing between the films was 0·16–0·24 mm. The simultaneously taken topographs are numbered in increasing order of the specimen-to-film distance, z_d, as $T1$, $T2$ *etc.* In the topographs, white contrast indicates higher intensity. A careful examination of Fig. 1 reveals that the fringe pattern varies slightly among topographs $T1$–$T4$. This can be observed on both edges of the fringe pattern. For example, the extreme left fringe (white contrast indicated by an oblique arrow) on line $Y=-1$ terminates on this line in $T2$, while it extends to a slightly lower position in $T4$. Also, the extreme right fringe on $Y=-2$ extends to a lower position in $T2$ and $T3$ than in $T1$ and $T4$.

Fig. 2 shows a set of microphotometer traces measured along line $Y=-1$ on the seven topographs mentioned. The illuminated area at the measured points was 10 μm (the X direction) × 200 μm (the Y direction). 18 intensity peaks (corresponding to white fringes in Fig. 1) are observed and numbered at the top of the figure. Although most fringe profiles deviate from the regular sinusoidal shape, we assume that the peak of the profiles gives the fringe position. For profiles with a split peak, the midpoint between the subpeaks is taken as the fringe position. Then it is seen that an oscillatory change of the fringe positions occurs among the topographs. The fringes showing the largest and the smallest changes are marked respectively by □ and ⊙. The positions of all other fringes also fluctuate to various extents.

Another remarkable feature of Fig. 2 is that the profiles of individual fringes vary in an unusual manner among topographs $T1$–$T7$. For example, the peaks of fringes 2–4 rise and fall against one another amongst the topographs. To show this clearly, peak heights measured from the density level on the extreme left edge are given on an arbitrary scale for some fringes. The zero level employed here is close to the photographic background level, but is raised somewhat in trace $T5$ for an unknown reason. The lateral widths of fringe profiles also vary in an oscillatory manner. It is noteworthy that the decrease (or increase) in the peak height is accompanied by the increase (or decrease) in the lateral width, and thus these two changes appear to correlate with each other (*e.g.* see profiles nos. 14 and 16 on traces $T1$ and $T2$). It should be stressed that the profile change as described above is inconsistent with the ordinary intensity attenuation by film absorption.

Microphotometer traces were measured every 1 mm on the Y axis on the topographs. Changes in the fringe position and profile like those in Fig. 2 were observed on every measured Y position. Correlation between different Y positions in these changes was not found. The reason for the lack of correlation could possibly be that the distance of 1 mm exceeds a characteristic correlation length.

Fringe positions determined from the microphotometer traces in Fig. 2 are plotted on a horizontal plane in Fig. 3, so as to give a general view of the nonprojective behavior of moiré fringes. The fringe positions oscillate along the beam path with various amplitudes, in a similar way to the bicrystal moiré fringes (*cf.* Fig. 7 in Yoshimura (1989)]. The amplitude of oscillation is 10 to 50% of the mean fringe spacing (=0·25 mm) in this case.

The half widths of rocking curves measured from various areas on the analyzer wafer of the X-ray interferometer were 1·28–1·38″ for a moiré pattern similar to Fig. 1. The

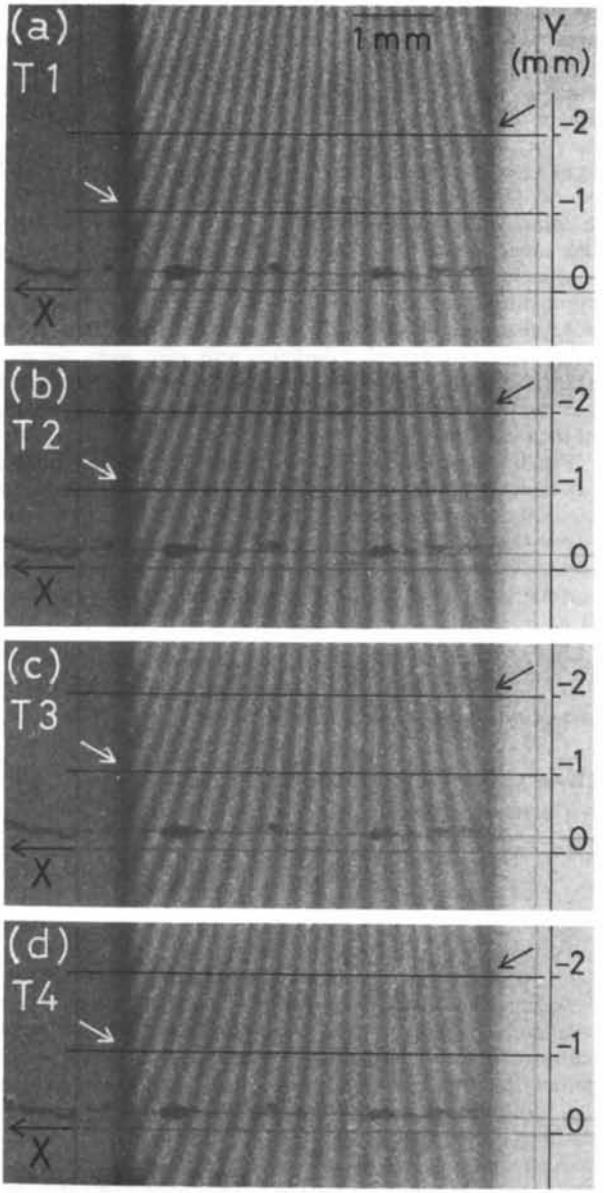

Fig. 1. Moiré patterns obtained with the X-ray interferometer by simultaneously photographing on parallel X-ray films. Transmitted-wave images. The X-ray beam was incident on the films at 10° off the film normal. (*a*) $T1$, $z_d=32{\cdot}2$ mm; (*b*) $T2$, $z_d=32{\cdot}4$ mm; (*c*) $T3$, $z_d=32{\cdot}6$ mm; (*d*) $T4$, $z_d=32{\cdot}8$ mm. Two vertical and one horizontal (the lower one) linear images are the shadows of thin Pt wires mentioned in the text. The X axis is taken on the horizontal linear image. Another horizontal linear image (the upper one) is the shadow of a Pt wire suspended on the exit surface of the analyzer wafer in order to give position markers on the specimen. Horizontal lines are drawn at $Y=-1$ and $Y=-2$ mm for easy comparison of the fringe patterns.

obtained values of the half width are close to the value expected from a perfect crystal. This result confirms that no great lattice distortion was present in the specimen. Therefore, by the same argument as before (Yoshimura, 1989), the observed change in fringe position cannot be explained by lattice distortion.

It can safely be presumed that the nonprojectiveness, *i.e.* the fringe oscillation, of the present moiré fringes is of the same nature as that of the previous bicrystal moiré fringes. The change in fringe profile found in the present study shows that moiré fringes are nonprojective not only in their positions and directions, but also in their intensity profiles.

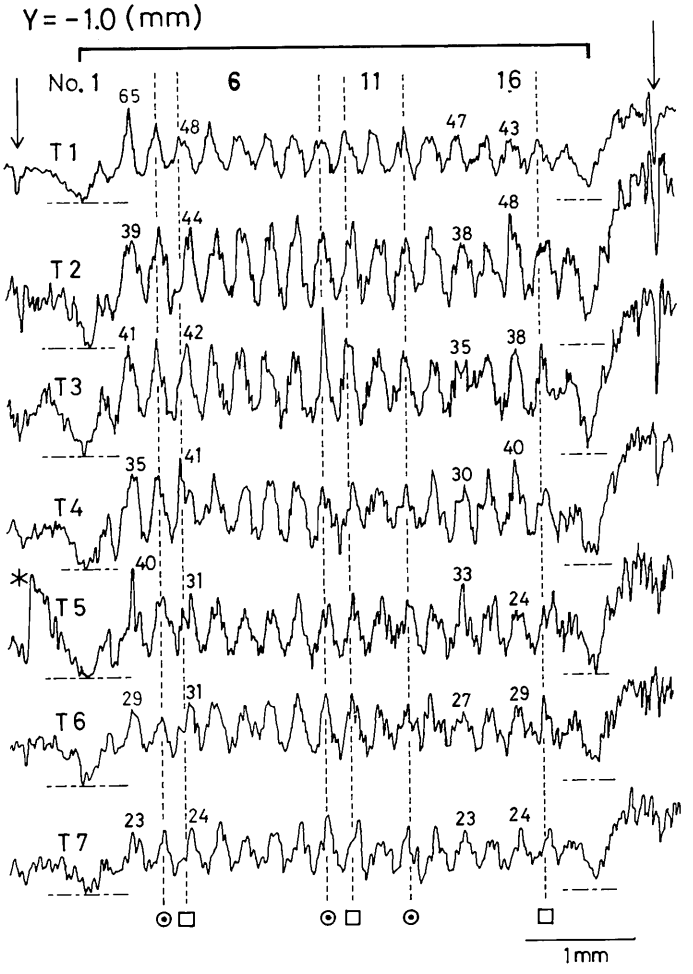

Fig. 2. Microphotometer traces of moiré fringes on the same set of topographs as in Fig. 1, measured along line $Y = -1$. Figures at the top give fringe numbers. Two-digit figures give the peak heights of profiles. Arrows indicate the positions of the vertical linear images used as positional standards. Horizontal dash-dotted lines indicate the zero density levels in the peak-height measurement. The vertical scale for $T1$ is reduced to one half of those for the other traces. The intensity enhancement marked * is due to a carelessly introduced scratch on the X-ray film.

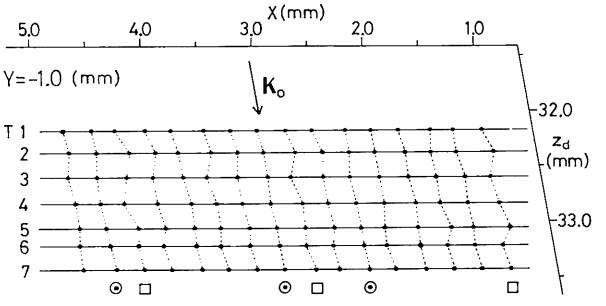

Fig. 3. Plots of the fringe positions determined from the microphotometer traces in Fig. 2. The arrow indicates the direction of the beam path.

This unusual profile change evidences the abnormality of the wave field which involves the interference of moiré fringes. The origin of the nonprojectiveness is not yet clear.

The author thanks Professor M. Ando and Dr P. Spieker of the Photon Factory, KEK, Tsukuba, and Dr K. Nakayama of the National Research Laboratory of Metrology, Tsukuba, for their help and advice in fabricating the X-ray interferometer. The author thanks Konica Corporation for permission to use a microphotometer.

References

BONSE, U. & HART, M. (1965). *Appl. Phys. Lett.* **6**, 155–156.
YOSHIMURA, J. (1987). *Acta Cryst.* A**43**, C221.
YOSHIMURA, J. (1989). *J. Phys. Soc. Jpn*, **58**, 1283–1295.